Inorganic Chemistry

Article

pubs.acs.org/IC

Modulation of the Magnetic Properties of Two-Dimensional Compounds [NiX_2(N−N)] by Tailoring Their Crystal Structure

Miguel Cortijo,[†] Santiago Herrero,*[,†] Reyes Jiménez-Aparicio,*[,†] and Emilio Matesanz[‡]

[†]Departamento de Química Inorgánica and [‡]Centro de Asistencia a la Investigación de Difracción de Rayos X, Facultad de Ciencias Químicas, Universidad Complutense de Madrid, Ciudad Universitaria, 28040 Madrid, Spain

Supporting Information

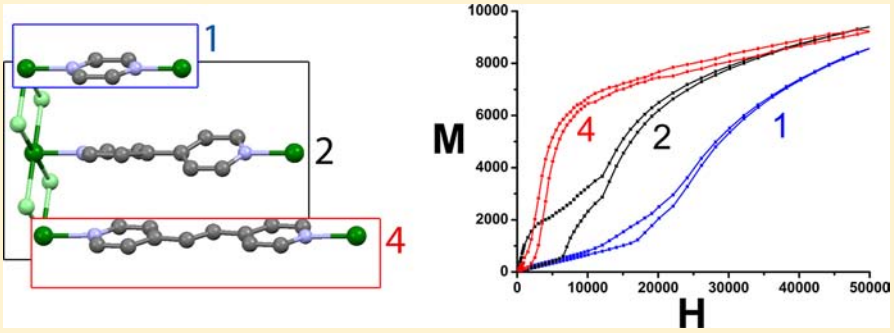

ABSTRACT: A series of 2-D nickel compounds with the stoichiometry [$NiCl_2$(N−N)] has been prepared, [N−N = pyrazine (**1**), 4,4′-bipyridine (**2**), *trans*-4,4′-azopyridine (**3**), *trans*-1,2-bis(4-pyridyl)ethylene (**4**), and 1,2-bis(4-pyridyl)ethane (**5**)]. The complex [$NiBr_2$(4,4′-bpy)] (**6**) was also obtained for comparative reasons. Compound **2** is the β phase of the previously reported complex [$NiCl_2$(4,4′-bpy)]. The syntheses of complexes **1**−**6** were carried out using solvothermal and microwave techniques. The compounds have been characterized by elemental analysis, infrared spectroscopy, thermogravimetry, and powder X-ray diffraction. The crystal structures of compounds **1**, **4**, and **5** have been solved using ab initio X-ray powder diffraction methods. Compounds **1**−**6** show the same arrangement, and their structures are described as layers formed by [NiX_2] chains linked perpendicularly by N−N ligands. The magnetic properties of the compounds are explained as a balance between the ferromagnetic interactions along the [NiX_2] chains and the antiferromagnetic interactions between chains from different layers. This work demonstrates that this balance can be tuned by the length of the N−N ligand.

INTRODUCTION

Polymeric structures, such as coordination polymers (CPs) and metal−organic frameworks (MOFs), are systems based on metallic nodes interconnected by different ligands propagated infinitely in one, two, or three dimensions and are being intensively studied because of their numerous potential applications.[1,2] The properties of polymeric structures are dependent on the chemical nature of their building blocks and the molecular and/or intermolecular forces that describe their extended structures.[1] Of special importance is the nature of the bridging ligand because it allows a certain amount of control of the assembly process. In particular, 2-D coordination polymers[3] have potential applications in different areas such as electrical conductivity, magnetism, gas storage, and catalysis but have been less studied than 1-D and 3-D compounds. Two-dimensional CP systems have some similarities to graphene, and this fact has also promoted the development of this class of materials.[3−6]

The synthesis and characterization of this type of compound constitute one of the most exciting challenges in recent chemistry.[2] The control of the reaction conditions to obtain materials with predefined structures and desired physicochemical properties is the basis for crystal-engineering techniques that constitute a fascinating and constantly growing field in chemistry. We aim to apply these concepts to the preparation of 2-D nickel compounds.

Because octahedral Ni(II) ions are paramagnetic, they are appropriate for synthesizing compounds with the magnetic properties of interest. A simple 2-D array containing Ni(II) ions can be obtained using halides and 4,4′-bipyridine (4,4′-bpy) as linkers. Thus, some 2-D compounds with a formula of [NiX_2(4,4′-bpy)] (X = Cl and Br) were published many years ago,[7−10] and their crystal structures were solved with ab initio X-ray powder diffraction.[8] The magnetic properties of the 2-D compounds [MCl_2(4,4′-bpy)] (M = Fe, Co, Ni, and Co/Ni) have also been studied and show the existence of spontaneous magnetic ordering and metamagnetic transitions. A low-temperature neutron-diffraction study of [$NiCl_2$(4,4′-bpy-d_8)] has shown[11] that in this complex the nickel ions are ferromagnetically coupled within the metal−chloride chains and these chains are antiferromagnetically coupled. Taking into account these antecedents, we have tried to extend the series [$NiCl_2$(N−N)] by changing the nature of the N−N connectors

Received: March 14, 2013
Published: May 29, 2013

   dx.doi.org/10.1021/ic400632c | *Inorg. Chem.* 2013, 52, 7087−7093

while maintaining the same basic structure to establish the influence of the organic linkers on the antiferromagnetic coupling. In this way, we could modulate the ferromagnetism in these complexes. Thus, in this work we describe the preparation of a series of 2-D compounds with general formula $[NiCl_2(N{-}N)]$ [N−N = pyrazine (pyz), *trans*-4,4′-azopyridine (*t*-apy), *trans*-1,2-bis(4-pyridyl)ethylene (*t*-bpee), and 1,2-bis(4-pyridyl)ethane (bpe)] (Figure 1). A new phase (β) of the

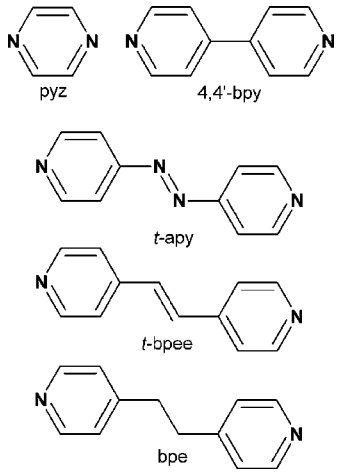

Figure 1. N,N′-Donor ligands employed in the present work.

previously reported $[NiCl_2(4,4'\text{-bpy})]$ compound is also described. The synthesis of the complex $[NiBr_2(4,4'\text{-bpy})]$ has also been carried out for comparative purposes. The influence of the halide ligands and the N,N-donor ligands on the ferro- and antiferromagnetic properties of these 2-D compounds is analyzed.

EXPERIMENTAL SECTION

General Comments and Physical Measurements. Solvothermal syntheses were carried out with a Memmert Universal Oven UFE 400 using Teflon-lined stainless-steel autoclaves. Microwave-assisted solvothermal reactions were carried out with an ETHOS One microwave oven using TFM Teflon closed vessels equipped with a temperature sensor and pressure controller. FTIR spectra (4000−650 cm^{-1}) were recorded with a Perkin-Elmer Spectrum 100 with a universal ATR accessory. Low-frequency IR spectra and elemental analyses were carried out by the Spectroscopy and Microanalytical Services of the Universidad Complutense de Madrid.

Thermogravimetric analyses were performed under nitrogen and in an air atmosphere at up to 1000 °C, with a heating rate of 5 °C·min^{-1} using a Perkin-Elmer Pyris 1 TGA instrument. The variable-temperature magnetic-susceptibility data were obtained with a Quantum Design MPMSXL SQUID (Superconducting Quantum Interference Device) magnetometer over a temperature range of 2−300 K. All data were corrected for the diamagnetic contribution of both the sample holder and the compound to the susceptibility. The molar diamagnetic corrections for the complexes were calculated on the basis of Pascal's constants.

Synthesis. Reactants and solvents were used as received. All products were obtained either by solvothermal or microwave-assisted solvothermal synthesis by the reaction of a nickel(II) halide ($NiCl_2{\cdot}6H_2O$ or $NiBr_2{\cdot}3H_2O$) and a N,N′-donor ligand in a molar ratio of 1:1.

General Procedure for the Solvothermal Synthesis of Compounds of the Type $[NiCl_2(N{-}N)]$ (N−N = pyz, 4,4′-bpy, t-apy, t-bpee, and bpe) and $[NiBr_2(4,4'bpy)]$. A mixture of 1.25 mmol of $NiX_2{\cdot}nH_2O$, 1.25 mmol of N−N bidentate ligand, 9 mL of ethanol, and 3 mL of water was sealed in a Teflon-lined stainless-steel autoclave. The system was held at 120 °C for 1 day under autogenous pressure and afterward cooled slowly. The obtained solid was filtered, washed with 2 × 5 mL of ethanol and 2 × 5 mL of diethyl ether, and dried under vacuum.

General Procedure for the Microwave Synthesis of Compounds of the Type $[NiCl_2(N{-}N)]$ (N−N = pyz, 4,4′-bpy, t-apy, t-bpee, and bpe) and $[NiBr_2(4,4'bpy)]$. Equal quantities of the same reactants and solvents that were used in general procedure A were placed into an 85 mL Teflon vessel with a magnetic stirrer. The vessel was sealed with a lid equipped with a temperature sensor and placed in the microwave oven. The reaction mixture was held for 3 h at 120 °C and left to cool afterward. The solid was also isolated by following the same method that was used in the general procedure for solvothermal synthesis.

Structural Analysis. X-ray powder diffraction scans were recorded with a Panalytical X'Pert PRO diffractometer in reflection mode. A Ge(111) primary-beam monochromator (Cu $K\alpha_1$ radiation, λ = 1.5406 Å) was used together with a fixed divergence slit in the incident beam optics. The diffracted-beam optics consisted of an X'Celerator fast detector. Scans were collected with a 0.017° step size in the range of 2θ = 5−120° (compounds **1** and **2**) or 2θ = 5−100° (compounds **3**−**6**). Diffractograms for chlorido compounds **1**, **2**, **4**, and **5** were indexed with the DICVOL[12] and TREOR[13] programs as included in the Panalytical B.V. X'PertHighScore software. Proposed space groups were also determined with the help of this software. In the refinement of **2**, the atomic coordinates of an isomorphic compound were used as the starting data.[11] Structures **1**, **4**, and **5** were determined ab initio using the FOX program.[14] To find a suitable model to be used in FOX as a rigid body, a search of the CSD database[15] was done for each organic moiety. CSD entry SARTEK01[16] was used to obtain the pyrazine ring model for compound **1**. The *trans*-1,2-bis(4-pyridyl)-ethylene ligand for compound **4** was modeled with the corresponding atomic coordinates from entry WEHVIP.[17] For **5**, the 1,2-bis(4-pyridyl)ethane moiety was loaded into FOX with the coordinates of the flat molecule that are present in CSD entry YIDQOS.[18]

The structural models obtained with FOX were refined using the Rietveld method[19] with Fullprof software.[20] Hydrogen atoms were not considered in the model, and only the B overall temperature factor was refined for every compound. Anisotropic broadening of the peaks was found in the X-ray diffraction scans of compounds **1**, **2**, **4**, and **5**. Therefore, peak profiles also had to be refined for this effect to get a better fit. Except for compound **1**, the refinements were carried out by applying restraints to bond distances and angles of the organic moieties.

The diffractogram with the Rietveld fit of compound **1** is shown in Figure 2. The rest of the diffractograms are included in the Supporting Information (Figure S2). The diffractogram of complex **6** was found to be identical to that already described in the literature.[8] This point was confirmed by the good agreement obtained with a Le Bail fit,[21] and

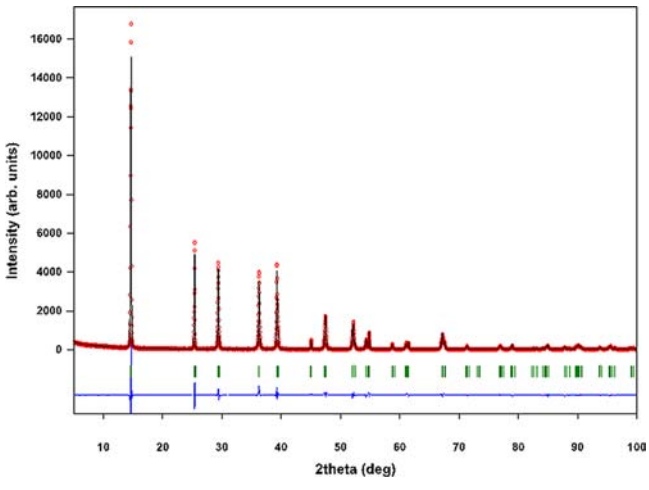

Figure 2. Diffractogram of compound **1** with its Rietveld fit.

dx.doi.org/10.1021/ic400632c | Inorg. Chem. 2013, 52, 7087−7093

Table 1. Yield, Elemental Analysis, and IR Absorptions for Compounds 1−6 under Conventional Solvothermal (S) and Microwave-Assisted (MW) Conditions

compound	method	yield (%)	C (%)[b]	H (%)[b]	N (%)[b]	IR bands (cm^{-1})[c]
$[NiCl_2(pyz)]$ (**1**)[a]	S	80	22.48	1.92	13.20	3322br, 3120w, 1912w, 1484m, 1413s, 1170s, 1116s, 1059s, 787s
	MW	85	22.40 (22.43)	2.02 (2.12)	13.15 (13.08)	
$[NiCl_2(4,4'\text{-bpy})]$ (**2**)	S	83	41.99	2.97	9.93	3063w, 1609s, 1535m, 1493m, 1414s, 1220s, 1081m, 1049w, 1012m, 855m, 811s, 729m
	MW	78	41.96 (42.03)	2.82 (2.82)	9.94 (9.80)	
$[NiCl_2(t\text{-apy})]$ (**3**)[a]	S	83	37.60	2.61	17.56	3370br, 3064w, 1601s, 1570m, 1490m, 1416s, 1228s, 1048m, 1018m, 820f, 568s
	MW	84	37.75 (37.73)	2.58 (2.69)	17.67 (17.60)	
$[NiCl_2(t\text{-bpee})]$ (**4**)	S	86	46.22	3.23	8.98	3061w, 3042w, 1609 s, 1562w, 1506m, 1425s, 1356w, 1305w, 1258w, 1206m, 1079w, 1021s, 983s, 968s, 847m, 824s, 747w
	MW	84	45.99 (46.24)	3.26 (3.40)	9.06 (9.08)	
$[NiCl_2(bpe)]$ (**5**)	S	66	45.84	3.84	8.96	3063w, 2930w, 1616s, 1561w, 1508m, 1437s, 1423s, 1347w, 1284w, 1218m, 1081w, 2025m, 820s, 682m
	MW	75	45.76 (45.92)	3.81 (3.85)	9.05 (8.93)	
$[NiBr_2(4,4'\text{-bpy})]$ (**6**)	S	78	32.04	2.26	7.51	3070w, 1607s, 1534m, 1490m, 1407s, 1218s 1078s, 1048w, 1008m, 850w, 799s, 723m
	MW	90	32.61 (32.05)	2.39 (2.15)	7.71 (7.48)	

[a]Elemental analysis was calculated with 0.25 water molecules. [b]Calculated analyses in parentheses. [c]Figure S1 (Supporting Information) for the IR spectra of **1**−**6**.

consequently no further structural analysis was done with this compound. Structural CIF files have been deposited in the CCDC (nos. CCDC 926 261−926 264). These data can be obtained free of charge from The Cambridge Crystallographic Data Centre via www.ccdc.cam.ac.uk/data_request/cif.

RESULTS AND DISCUSSION

Synthesis of the Compounds. Compounds $[NiCl_2(N-N)]$ (**1**−**5**) were prepared using five N,N′-donor ligands (Figure 1): pyrazine (**1**), 4,4′-bipyridine (**2**), *trans*-4,4′-azopyridine (**3**), *trans*-1,2-bis(4-pyridyl)ethylene (**4**), and 1,2-bis(4-pyridyl)ethane (**5**). $[NiBr_2(4,4'\text{-bpy})]$ (**6**) was also obtained. The reactivity of $NiCl_2{\cdot}6H_2O$ with 1,2-bis(4-pyridyl)-propane and 4,4′-dithiopyridine was also explored. Unfortunately, all of the attempts that were made with these last ligands gave compounds with stoichiometries of $[NiCl_2(N-N)_2]{\cdot}nH_2O$[22] and $[NiCl_2(N-N)_2]$, respectively.

The synthesis of compounds $[NiX_2(4,4'\text{-bpy})]$ (X = Cl, Br) (**2** and **6**) at room temperature in alcohol, water, or in a mixture of both solvents has been previously described,[8−10] although single crystals of these compounds were not obtained. It is well known that solvothermal methods are very effective at promoting crystal growth because in superheated solvents the viscosity decreases significantly, which increases the solubility and the diffusion rate of the reagents, leading to the improvement of crystal growth. This procedure had been successfully used to obtain single crystals of the compounds $[MCl_2(4,4'\text{-bpy})]$ (M = Fe, Co).[7]

To obtain single crystals in situ using solvothermal synthesis, numerous attempts under different conditions have been carried out. An additional reason to employ solvothermal synthesis is that the high temperatures reached in this method favor the formation of pure phases, avoiding a possible mixture of polymorphs as was found for $[CuCl_2(4,4'\text{-bpy})]$.[8] Different temperatures, reaction times, cooling rates, reactant concentrations, and diffusion reactions were explored to obtain single crystals of the compounds. Although no single crystal could be obtained because of the very low solubility of these polymeric complexes, very pure polycrystalline phases were isolated for all of the compounds. Moreover, they were obtained in high yields, except for compound **5** (Table 1). We had observed previously[23] that microwave-assisted solvothermal synthesis is even better for obtaining single-phase compounds and also saves time and energy. Therefore, compounds **1**−**6** were also synthesized using the microwave-assisted method, which requires only 2 h in contrast to the conventional solvothermal synthesis that requires 24 h.

Thermal Stability in Air. Compounds **1**−**6** decompose at high temperatures to form nickel(II) oxide (Figure S3 in the Supporting Information). The identity of the oxide was confirmed by powder X-ray diffraction (Figure S4 in the Supporting Information). Compounds **2**, **3**, **4**, and **6** are thermally stable up to 460, 375, 435, and 460 °C, respectively, and their thermogravimetric curves basically display this sole weight loss. However, compounds **1** and **5** show a two-step decomposition process. The first weight loss corresponds to the formation of $NiCl_2$ and $NiCl_2(bpe)_{0.5}$ at 380 and 330 °C for **1** and **5**, respectively. The heating of these intermediate species gives rise to NiO at 485 and 475 °C (Table 2 and Figure S3 in the Supporting Information).

Table 2. Weight Loss Observed for Compounds 1−6 in Their Thermogravimetric Curves and Tentative Assignments of the Formed Species

	weight loss T (°C)	product formed	theoretical loss (%)	experimental loss (%)
1	380	$NiCl_2$	38.2	39.5
	485	NiO	64.4	64.5
2	460	NiO	73.9	74.0
3	375	NiO	76.0	77.6
4	435	NiO	76.0	75.8
5	330	$NiCl_2(bpe)_{0.5}$	29.2	28.2
	475	NiO	76.2	76.5
6	460	NiO	80.0	81.5

When the thermogravimetric studies of compounds **2** and **6** were carried out under a nitrogen atmosphere, in both cases a two-step pattern was observed, and the final product was metallic nickel.[7,8]

Description of the Structures. Crystal structures of **1**, **2**, **4**, and **5** were solved using X-ray powder diffraction methods. Crystal data of compounds **1**, **2**, **4**−**6** are listed in Table 3. The parameters of the previously reported phase α-$[NiCl_2(4,4'\text{-bpy})]$[8] have also been included for comparison. All of the compounds crystallize in an orthorhombic space group, with the exception of compound **5**, which crystallizes in a monoclinic space group.

dx.doi.org/10.1021/ic400632c | Inorg. Chem. 2013, 52, 7087−7093

Table 3. Crystal Data of $[NiCl_2(pyz)]$ (1), β-$[NiCl_2(4,4'\text{-bpy})]$ (2), α-$[NiCl_2(4,4'\text{-bpy})]$, $[NiCl_2(t\text{-bpee})]$ (4), $[NiCl_2(bpe)]$ (5), and $[NiBr_2(4,4'\text{-bpy})]$ (6)

	1	2	α-$[NiCl_2(4,4'\text{-bpy})]$	4	5	6
space group	*Cmmm*	*Pban*	*Cmmm*	*Pnnm*	*P21/a*	*Cmmm*
a (Å)	12.04909(15)	11.94192(9)	11.9822(9)	11.78396(18)	11.71243(17)	12.40928(9)
b (Å)	7.00406(9)	11.31702(7)	11.3196(6)	13.56871(17)	13.58998(15)	11.33290(6)
c (Å)	3.51307(5)	3.58496(2)	3.5830(3)	3.61331(5)	3.67828(9)	3.73954(3)
β (deg)					97.629(4)	
V (Å^3)	296.477(7)	484.497(6)	485.98(6)	577.744(14)	580.296(17)	525.904(6)
ρ_{calc}/ g·cm^{-3}	2.349	1.959	1.953	1.792	1.796	2.366
Z	2	2	2	2	2	2
fw	209.680	285.783	285.783	311.821	313.836	374.685
ref. method	Rietveld	Rietveld		Rietveld	Rietveld	Le Bail
Rp	9.94	9.58		8.22	9.29	5.64
Rwp	12.9	12.7		11.3	12.9	7.55
χ^2	2.05	2.31		3.17	4.06	2.40
Rb	4.81	5.82		4.70	5.89	
Rf	5.09	3.71		5.30	3.39	

The replacement of N−N ligands in the structure of $[NiCl_2(N-N)]$ compounds mainly affects the value of the *b* parameter because these ligands connect nickel centers in the [010] direction. Thus, chlorido derivatives (**1**, **2**, α-$[NiCl_2(4,4'\text{-bpy})]$, **4**, and **5**) show increasing values of this parameter. Moreover, there is a linear relationship between the *b* parameter of the cell and the distance between the N-donor atoms of the bidentate ligands (angstroms): $b = 4.25888 + 0.99365 \times d(N\cdots N)_{ligand}$ ($R^2 = 0.99996$). The *c* parameter also slightly increases and the *a* parameter slightly decreases with the increasing length of the N−N ligand. Compounds **2** and **6**, with the same N−N ligand, present a similar value for *b*. However, the *a* and *c* parameters increase significantly when chloride is replaced by bromide.

In all cases, the Ni(II) centers exhibit an octahedral environment formed by four chloride ligands and two nitrogen atoms in a trans disposition. N−N bidentate ligands connect nickel centers along the *b* direction, whereas chloride ligands bridge nickel atoms along the *c* direction, generating a layer (Figure 3). The longer the N-donor ligand is, the farther the

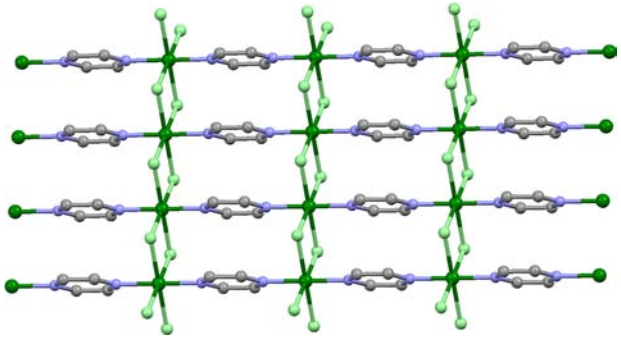

Figure 3. Drawing of a *bc* layer of $[NiCl_2(pyz)]$ (**1**).

distance between Ni atoms in the *b* direction and also the distance between Ni atoms bridged by chloride ligands in the *c* direction. The Ni−Cl−Ni angle also increases with the length of the N−N ligand (Table 4).

Layers are packed in the [100] direction for compounds **1**, **2**, **4**, and **6**. The longer the N−N ligand is, the farther the distance between nickel centers from contiguous layers (Table 4). As an

Table 4. Selected Distances (Angstroms) and Angles (Degrees) for Compounds 1, 2, 4−6

	shortest *d*(Ni···Ni) (Å)			
compound	*b* direction	*c* direction	interlayer	Ni−X−Ni angle (deg)
1	7.004	3.513	6.968	92.64
2	11.317	3.585	8.226	93.95
4	13.569	3.613	9.166	94.13
5	13.590	3.678	8.970	95.18
			9.396	
6	11.330	3.734	8.397	92.02

illustration of the stacking, two layers of compound **4** are shown in Figure 4.

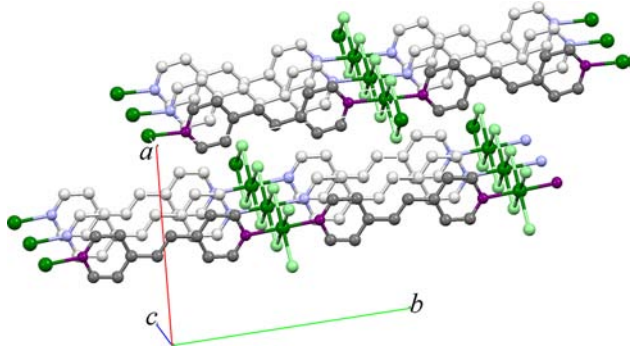

Figure 4. Drawing of two layers of $[NiCl_2(t\text{-bpee})]$ (**4**).

The arrangement of the layers in compound **5** is slightly different than that in the rest of the compounds, as is shown in Figure 5.

Structures of complexes **2** and **6** have already been reported[8] and were also based on powder X-ray diffraction analysis. Diffractograms of compound **6** and $[NiBr_2(4,4'\text{-bpy})]$ are indistinguishable (Figure S2 in the Supporting Information). Therefore, complex **6**, which was obtained from solvothermal methods, and the previously described are the same. However, chlorido derivative **2** described in this work presents a slightly different powder X-ray diffraction pattern than the pattern previously reported for $[NiCl_2(4,4'\text{-bpy})]$. We have determined the structure of **2** by X-ray powder diffraction methods. The

dx.doi.org/10.1021/ic400632c | *Inorg. Chem.* 2013, 52, 7087−7093

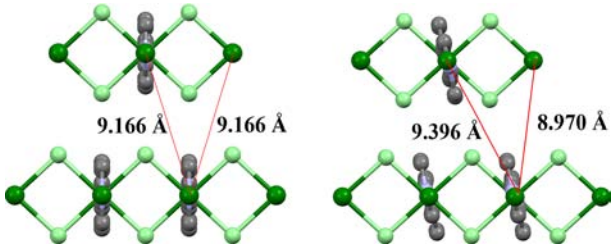

Figure 5. View along the *b* axis of $[NiCl_2(t\text{-bpee})]$ (**4**) (left) and $[NiCl_2(bpe)]$ (**5**) (right).

difference is due to a different disposition of the aromatic rings in the 4,4′-bpy ligand, which are not situated on the same plane (Figure 6). This disposition was already found for $[NiCl_2(4,4'\text{-bpy-}d_8)]$.[11] In fact, coplanar and noncoplanar aromatic rings in 4,4′-bpy have been observed for other $[MX_2(4,4'\text{-bpy})]$ compounds (M = Mn, Fe, Co, Cu, Zn, Cd, and Hg; X = Cl, Br, and I).[8,24] However, only very few compounds are known that have both conformations: $[CdX_2(4,4'\text{-bpy})]$ (X = Br, I)[24] or $[CuCl_2(4,4'\text{-bpy})]$.[8] Moreover, the monoclinic phase of *β*-$[CuCl_2(4,4'\text{-bpy})]$ is formed from orthorhombic *α*-$[CuCl_2(4,4'\text{-bpy})]$ with time or by applying pressure because *β* is more dense than *α* (1.911 and 1.908 g/cm^3, respectively). In compound **2**, phase *β*-$[NiCl_2(4,4'\text{-bpy})]$ is also slightly more dense (1.959 g/cm^3) than the *α* phase[8] (1.953 g/cm^3). This *β* phase could also be the thermodynamically most stable phase because it was obtained under solvothermal conditions. This is in accordance with the fact that the previously reported *α* phase of $[NiCl_2(4,4'\text{-bpy})]$[8] was prepared at room temperature. It is noteworthy that although the *α* phase was also initially proposed for a compound obtained under solvothermal conditions[7] the same authors assumed later that the compound was *β*-$[NiCl_2(4,4'\text{-bpy})$ on the basis of neutron diffraction studies.[11]

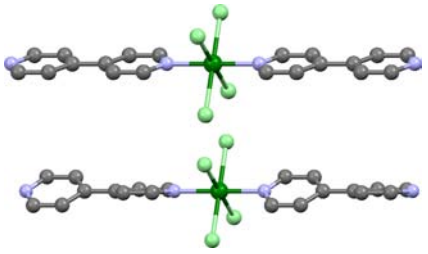

Figure 6. Coordination environment of the Ni centers for *α*-$[NiCl_2(4,4'\text{-bpy})]$ (top) and *β*-$[NiCl_2(4,4'\text{-bpy})]$ (**2**) (down) showing the conformations of their aromatic rings.

The diffractogram obtained for compound **3** is reminiscent of those for compounds **2** and **4** (Figure S2 in the Supporting Information). However, the reflections were not indexed because of the presence of wide peaks, probably resulting from a disordered stacking of the layers. Moreover, the low-frequency IR spectrum of **3** is similar to that reported in the literature for $[NiCl_2(4,4'\text{-bpy})]$ in the region where *ν*(Ni−Cl) and *ν*(Ni−N) are expected.[9] This fact points to the same nickel-coordination environment for the two compounds (Figure 7).

Magnetic Properties. Because ferromagnetic superexchange is expected via the chlorido bridges in the chains of compounds **1**−**5**,[7,11] magnetization measurements versus magnetic field have been carried out. The representation of

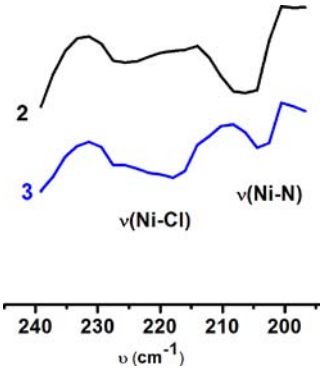

Figure 7. Low-frequency IR for *β*-$[NiCl_2(4,4'\text{-bpy})]$ (**2**) and $[NiCl_2(t\text{-apy})]$ (**3**).

the magnetization versus the magnetic field for compounds **1**−**5** at 2 K is depicted in Figure 8. In all cases, the representations

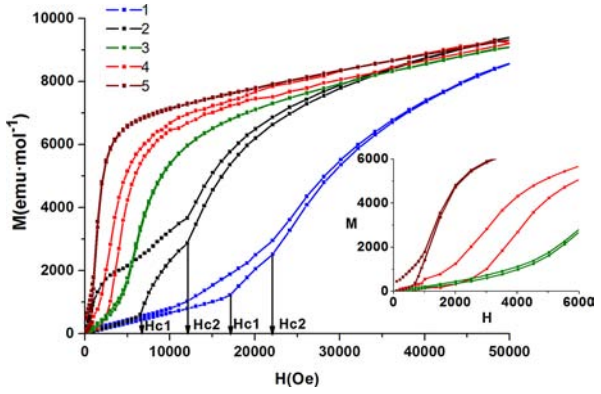

Figure 8. Magnetization vs field measured at 2 K for **1**−**5**. Inset: Low-field region for **3**−**5**.

from −5 T to 5 T show no reversibility under intermediate magnetic fields, which is especially appreciable for compound **2**, although the absence of remnant magnetization and coercivity (Figure S5 in the Supporting Information) rules out the existence of magnetic hysteresis at very low magnetic fields. Moreover, at very low magnetic fields, the $M(H)$ curves are linear, although for compound **1** the linearity is maintained until 17 kOe. This linearity is compatible with the presence of antiferromagnetic interactions that are corroborated with the magnetic data presented in Figure 9. However, the lack of reversibility at intermediate magnetic fields observed for all samples indicates the existence of additional complexity in the magnetic properties of these complexes. The plot of M versus H shows the metamagnetic behavior of these compounds. The presence of two critical magnetic fields (H_c) at 17 and 22 kOe for compound **1** and 6.5 and 12 kOe for compound **2** is indicated in Figure 8. A similar behavior was found in the magnetization curve for compound $[NiCl_2(4,4'\text{-bpy})]$.[7]

The representation of the magnetic susceptibility versus temperature under a very weak magnetic field (0.01 T, Figure 9) for all of the compounds shows a maximum, indicating predominant antiferromagnetism at very low temperatures. This maximum is observed at 10.2, 9.3, 7.9, 7.3, and 5.6 K for compounds **1**−**5**, respectively. At 0.01 T, the magnetic moment at room temperature for these compounds ranges from 4.17μ_B to 3.64μ_B. At higher magnetic fields (0.5, 1, and 5 T), the magnetic moments at room temperature are between 3.15μ_B

dx.doi.org/10.1021/ic400632c | Inorg. Chem. 2013, 52, 7087−7093

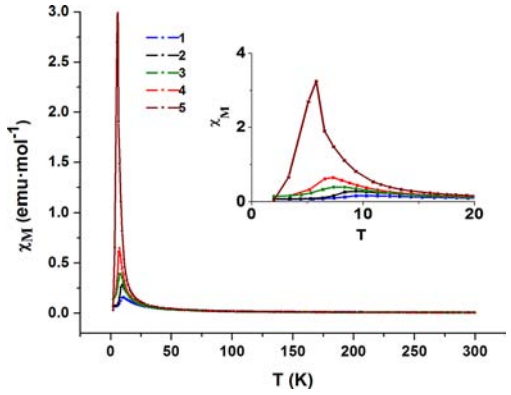

Figure 9. Magnetic susceptibility vs temperature measured at 0.01 T for compounds **1**–**5**. Inset: Low-temperature region.

and 3.51μ_B, which are very close to the typical values for Ni(II) complexes with spin–orbit coupling (Figure S6 in the Supporting Information).

The plot of the magnetic moment versus temperature of the chlorido derivatives is shown in Figure 10. The magnetic

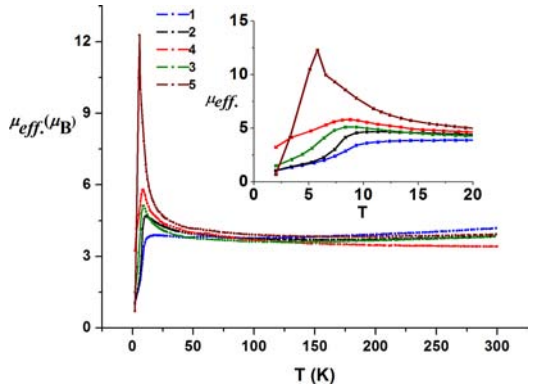

Figure 10. Magnetic moment vs temperature for chlorido derivatives **1**–**5** (0.01 T). Inset: Low-temperature region.

moment slowly decreases with decreasing temperature from room temperature to 100–150 K. From this point, the temperature values begin to increase until a maximum is reached, and afterward a fast decrease at very low temperatures is observed.

Thus, the magnetic measurements of compounds **1**–**5** demonstrate the presence of antiferromagnetic order and ferromagnetic interactions in all of the compounds. The antiferromagnetic ground-state magnetic structure changes into a ferromagnetic-like or paramagnetic-like ground state at stronger applied fields, in accordance with the magnetic properties described for the [$NiCl_2$(4,4′-bpy)] complex.[7] The most plausible explanation is that the first critical field separates the antiferromagnetic state and paramagnetic state because even at high fields the magnetization is still far from saturation (Figure 8).

The magnetic structure of [$NiCl_2$(4,4′-bpy-d_8)] demonstrated that the moments along the [MCl_2] chains are arranged ferromagnetically, and each of these chains is coupled antiferromagnetically to the nearest [MCl_2] chain, which belongs to another layer, giving a long-range antiferromagnetic-spin arrangement.[11]

Magnetic behavior of the analogous bromide compound **6** [$NiBr_2$(4,4′-bpy)] can be explained by considering that its magnetic structure is the same as that found for [$NiCl_2$(4,4′-bpy)]. However, the ferromagnetic interaction along the [$NiBr_2$] chains in **6** is lower than in **2** despite the similar X–Ni–X angle (92.02° instead of 93.95°). Lower ferromagnetic interactions in **6** are expected because the Ni–X distance is 0.149 Å longer for the bromido derivative. In Figure 11, the

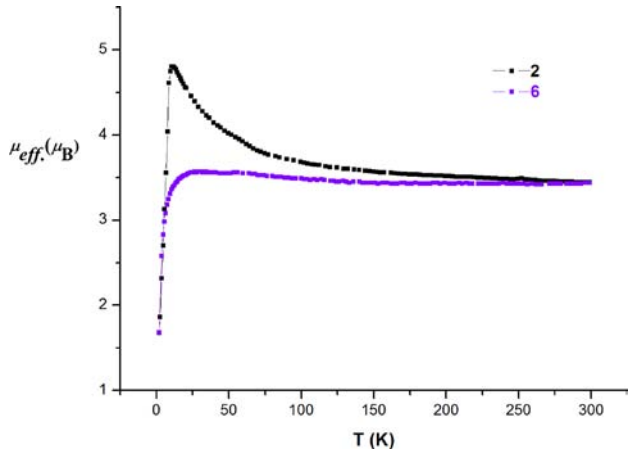

Figure 11. Magnetic moment vs temperature for **2** and **6** (0.5 T).

variation of the magnetic moment versus temperature for compounds **2** and **6** (at 0.5 T) is shown. Although in both curves a maximum is observed, the difference in the sharpness is very significant.

The comparison of the magnetic properties in **1**–**5** indicates that the most relevant feature is the correlation between the magnetic behavior and the size of the N–N ligand. The shorter the distance between the N-donor atoms in the ligand is, the higher the critical field (H_c) necessary to destroy the antiferromagnetic ground state. In other words, the shorter the ligand is, the stronger the antiferromagnetic exchange becomes. The magnetic interactions through 4,4′-bpy ligands were discarded in the magnetic structure analysis of [$NiCl_2$(4,4′-bpy-d_8)] because the distance between Ni atoms is too great. Therefore, the antiferromagnetic interactions between [$NiCl_2$] chains occur through space.[11] However, in compound **1**, an additional interaction through the short pyrazine ligand may take place, intensifying the antiferromagnetism in this compound.

Thus, the decrease in antiferromagnetism with the increase in ligand size in **1**–**4** could be explained by considering that the longer the N–N ligand, the farther the distance between the nickel centers from the nearest [$NiCl_2$] chains, which belong to contiguous layers (Table 4). Surprisingly, compound **5** is less antiferromagnetic than compound **4** despite the fact that the shortest interlayer Ni···Ni distance, which favors antiferromagnetic interactions, is shorter for compound **5**. However, it must be taken into account that each nickel center has eight nickel-interlayer neighboring atoms at 9.166 Å in compound **4**, whereas in compound **5** each nickel center has four at 8.970 Å and four at 9.396 Å (Figure 5).

■ CONCLUSIONS

Compounds [$NiCl_2$(N–N)] [N–N = pyrazine (**1**), 4,4′-bipyridine (**2**), *trans*-4,4′-azopyridine (**3**), *trans*-1,2-bis(4-pyridyl)ethylene (**4**), and 1,2-bis(4-pyridyl)ethane (**5**)] and

dx.doi.org/10.1021/ic400632c | Inorg. Chem. 2013, 52, 7087–7093

$[NiBr_2(4,4'\text{-bpy})]$ (**6**) can be prepared as single phase and in good yield under conventional solvothermal conditions. However, the microwave-assisted solvothermal method allows for reduced reaction times and saved energy with similar yields.

The replacement of the diamine ligand in $[NiCl_2(4,4'\text{-bpy})]$ by a shorter or longer above-mentioned N−N ligand does not affect the basic disposition of the ligands. All of the compounds show metamagnetic transitions. The ground state is antiferromagnetic at low applied magnetic fields and paramagnetic with ferromagnetic interactions at higher magnetic fields. Ferromagnetic interactions take place along the $[NiCl_2]$ chains, although there is no remnant magnetization and the coercivity is zero. Antiferromagnetism is generated from interlayer−space interactions among $[NiCl_2]$ chains. The longer the N−N ligand is, the farther the interlayer distance between $[NiCl_2]$ chains becomes for compounds **1**−**4**. Surprisingly, there is a significant decrease in the antiferromagnetic interaction in compound **5** with respect to that in compound **4**, even though they have similar ligands and very similar lengths. This apparent anomaly can be ascribed to the crystal symmetry of the compounds, which is orthorhombic for **4** (*Pmmm*) and monoclinic ($P2_1/a$) for **5**. In any case, as the length of the ligand is increased the contribution of the antiferromagnetic interactions to the global magnetic behavior diminishes.

Therefore, the magnetism of the compounds can be fine-tuned by selecting an appropriate N−N ligand. Finally, it is worth mentioning that the deposition of individual layers of these compounds on surfaces would open up the possibility of applying them to the construction of nanodevices. Work in this direction is being carried out by our research group.

■ ASSOCIATED CONTENT

Supporting Information

Infrared spectra of **1**−**6**, powder X-ray diffractograms of **2**−**6**, thermogravimetric weight loss curves of **1**−**6**, powder X-ray diffraction data for NiO obtained after the thermogravimetric measurement of **1** in air, magnetization versus magnetic field (from −5 T to 5 T) measured at 2 K for **1**−**5**, magnetic moments (μ_B) at room temperature measured at different magnetic fields for **1**−**5**, and X-ray crystallographic files (CIFs). This material is available free of charge via the Internet at http://pubs.acs.org.

■ AUTHOR INFORMATION

Corresponding Author

*E-mail: sherrero@quim.ucm.es (S.H.), reyesja@quim.ucm.es (R.J.-A.).

Author Contributions

This work was carried out through contributions of all authors.

Notes

The authors declare no competing financial interest.

■ ACKNOWLEDGMENTS

We are grateful for financial support from the Spanish Ministerio de Ciencia e Innovación (CTQ2011-23 066) and the Comunidad de Madrid (S2009/MAT-1467).

■ REFERENCES

(1) (a) Zhou, H.-C.; Long, J. R; Yaghi, O. M. *Chem. Rev.* **2012**, *112*, 673−1268. (b) Long, J. R; Yaghi, O. M. *Chem. Soc. Rev.* **2009**, *38*, 1201−1508. (c) Janiak, C. *Dalton Trans.* **2003**, 2701−2804.

(2) Stock, N.; Biswas, S. *Chem. Rev.* **2012**, *112*, 933−969.

(3) Sakamoto, J.; van Heijst, J.; Lukin, O.; Schluter, D. A. *Angew. Chem., Int. Ed.* **2009**, *48*, 1030−1069.

(4) Umeyama, D.; Horike, S.; Inukai, M.; Itakura, T.; Kitagawa, S. *J. Am. Chem. Soc.* **2012**, *134*, 12780−12785.

(5) Huang, L.; Han, L.; Zhu, D.; Chen, L.; Xu, Y. *Inorg. Chem. Commun.* **2012**, *21*, 80−83.

(6) (a) Gallego, A.; Hermosa, C.; Castillo, O.; Berlanga, I.; Gómez-García, C. J.; Mateo-Martí, E.; Martínez, J. I.; Flores, F.; Gómez-Navarro, C.; Gómez-Herrero, J.; Delgado, S.; Zamora, F. *Adv. Mater.* **2013**, *25*, 2141−2146. (b) Amo-Ochoa, P.; Welte, L.; González-Prieto, R.; Sanz Miguel, P. J.; J. Gómez-García, C. J.; Mateo-Martí, E.; Delgado, S.; Gómez-Herrero, J.; Zamora, F. *Chem. Commun.* **2010**, *46*, 3262−3264.

(7) Lawandy, M. A.; Huang, X.; Wang, R.-J.; Li, J.; Lu, J. Y.; Yuen, T.; Lin, C. L. *Inorg. Chem.* **1999**, *38*, 5410−5414.

(8) Masciocchi, N.; Cairati, P.; Carlucci, L.; Mezza, G.; Ciani, G.; Sironi, A. *J. Chem. Soc., Dalton Trans.* **1996**, 2739−2746.

(9) Ferraro, J. R.; Davis, K. C. *Inorg. Chim. Acta* **1969**, *3*, 685−688.

(10) Musgrave, T. R.; Mattson, C. E. *Inorg. Chem.* **1968**, *7*, 1433−1436.

(11) Feyerherm, R.; Loose, A.; Lawandy, M. A.; Li, J. *Appl. Phys. A: Mater. Sci. Process.* **2002**, *74*, S778−S780.

(12) Boultif, A.; Louër, D. *J. Appl. Crystallogr.* **2004**, *37*, 724−731.

(13) Werner, P. E.; Erikson, L.; Westdahl, M. *J. Appl. Crystallogr.* **1985**, *18*, 367−370.

(14) Favre-Nicolin, V.; Cerny, R. *J. Appl. Crystallogr.* **2002**, *35*, 734−743.

(15) Allen, F. H. *Acta Crystallogr.* **2002**, *B58*, 380−388.

(16) Pickardt, J.; Staub, B. *Z. Naturforsch., B: J. Chem. Sci.* **1997**, *52*, 1456−1460.

(17) Li, Z.-G.; Xu, J.-W.; Jia, H.-Q.; Hu, N.-H. *Acta Crystallogr.* **2006**, *C62*, m205−m207.

(18) Zhang, L.; Yu, J. *Acta Crystallogr.* **2007**, *E63*, m1759.

(19) (a) Rietveld, H. M. *Acta Crystallogr.* **1967**, *22*, 151−152. (b) Rietveld, H. M. *J. Appl. Crystallogr.* **1969**, *2*, 65−71.

(20) Rodríguez-Carvajal, J. *Physica B* **1993**, *192*, 55−69.

(21) Le Bail, A.; Duroy, H.; Fourquet, J. L. *Mater. Res. Bull.* **1988**, *23*, 447−452.

(22) Carlucci, L.; Ciani, G.; Moret, J. M.; Proserpio, D. M.; Rizzzoto, S. *Cryst. Growth Des.* **2009**, *9*, 5024−5034.

(23) (a) Cortijo, M.; Herrero, S.; Jiménez-Aparicio, R.; Perles, J.; Torralvo, M. J.; Torroba, J. *Eur. J. Inorg. Chem.* **2013**, 2580−2590. (b) Delgado, P.; González-Prieto, R.; Jiménez-Aparicio, R.; Perles, J.; Priego, J. L.; Torres, M. R. *Dalton Trans.* **2012**, *41*, 11866−11874. (c) Herrero, S.; Jiménez-Aparicio, R.; Perles, J.; Priego, J. L.; Saguar, S.; Urbanos, F. A. *Green Chem.* **2011**, *13*, 1885−1890. (d) Herrero, S.; Jiménez-Aparicio, R.; Perles, J.; Priego, J. L.; Urbanos, F. A. *Green Chem.* **2010**, *12*, 965−967.

(24) (a) Hu, C.; Li, Q.; Englert, U. *CrystEngComm* **2003**, *5*, 519−529. (b) Chen, W.-T.; Fang, X.-N.; Luo, Q.-Y.; Xu, Y.-P.; Duan, Y.-P. *Acta Crystallogr.* **2007**, *C63*, m398−m400. (c) Biradha, K.; Fujita, M. *J. Inclusion Phenom. Macrocyclic Chem.* **2001**, *41*, 201−208. (d) Zhu, H.-G.; Hu, H.-M.; Yu, Z.; Cai, H.; You, X.-Z. Personal communication, 2004, CCDC118 506. (e) Niu, Y.; Hou, H.; Zhu, Y. Personal communication, 2005, CCDC197 095. (f) Chen, W. T.; Wang, M.-S.; Liu, X.; Guo, G.-C.; Huang, J.-S. *Cryst. Growth Des.* **2006**, *6*, 2289−2300.